Monthly Notices
of the
ROYAL ASTRONOMICAL SOCIETY

MNRAS **437,** 3596–3602 (2014)
Advance Access publication 2013 November 28

doi:10.1093/mnras/stt2154

Counterrotating stars in simulated galaxy discs

David G. Algorry,[1]⋆ Julio F. Navarro,[2]† Mario G. Abadi,[1] Laura V. Sales,[3] Matthias Steinmetz[4] and Franziska Piontek[5]

[1]*Observatorio Astronómico de Córdoba and CONICET, Córdoba, X5000BGR, Argentina*
[2]*University of Victoria. Victoria, BC V8P5C2, Canada*
[3]*Max-Planck Institute for Astrophysics, Karl-Schwarzschild-Strasse 1, D-85740 Garching, Germany*
[4]*Astrophysikalisches Institut Potsdam, An der Sternwarte 16, D-14482 Potsdam, Germany*
[5]*Potsdam Institute for Climate Impact Research, Telegraphenberg A31, D-14473 Potsdam, Germany*

Accepted 2013 November 5. Received 2013 November 4; in original form 2013 September 3

ABSTRACT

Counterrotating stars in disc galaxies are a puzzling dynamical feature whose origin has been ascribed to either satellite accretion events or to disc instabilities triggered by deviations from axisymmetry. We use a cosmological simulation of the formation of a disc galaxy to show that counterrotating stellar disc components may arise naturally in hierarchically clustering scenarios even in the absence of merging. The simulated disc galaxy consists of two coplanar, overlapping stellar components with opposite spins: an inner counterrotating bar-like structure made up mostly of old stars surrounded by an extended, rotationally supported disc of younger stars. The opposite-spin components originate from material accreted from two distinct filamentary structures which at turn around, when their net spin is acquired, intersect delineating a 'V'-like structure. Each filament torques the other in opposite directions; the filament that first drains into the galaxy forms the inner counterrotating bar, while material accreted from the other filament forms the outer disc. Mergers do not play a substantial role and most stars in the galaxy are formed in situ; only 9 per cent of all stars are contributed by accretion events. The formation scenario we describe here implies a significant age difference between the co- and counterrotating components, which may be used to discriminate between competing scenarios for the origin of counterrotating stars in disc galaxies.

Key words: Galaxy: disc – Galaxy: formation – Galaxy: kinematics and dynamics – Galaxy: structure.

1 INTRODUCTION

Galaxy discs are rotationally supported systems that consist largely of stars in coplanar, nearly circular orbits. Although most discs also contain stars in counterrotating orbits, these typically belong to separate spheroidal components (a bulge or a halo) characterized by little or no net rotation and large orbital excursions from the disc plane. Stellar discs are the unmistakable result of dissipative collapse, where a gaseous component cools and settles on to a rotationally supported structure before turning gradually into stars. The spheroidal components, on the other hand, are thought to arise from merger events where existing stars have their orbits randomized by the fluctuating gravitational potential.

Infrequently, a population of stars with small vertical motions but that counterrotates relative to the prevailing spin is also detected through the presence of separate peaks in the line-of-sight velocity distribution (LOSVD) measured from high-resolution spectra. Counterrotating stars are sometimes confined to the inner regions of the galaxy, as is the case for the counterrotating bulge of NGC 7331 (Prada et al. 1996), but are also found on occasion to overlap the main disc component, as in NGC 5719 (Vergani et al. 2007; Coccato et al. 2011); NGC 7217 (Merrifield & Kuijken 1994); NGC 3593 (Bertola et al. 1996); and NGC 4550 (Rix et al. 1992; Rubin, Graham & Kenney 1992).

The origin of such populations is not well understood. An external origin has been predicated on the basis that counterrotating bulges are reminiscent of the dynamically decoupled cores present in some elliptical galaxies (Bender & Surma 1992; Carter, Thomson & Hau 1998; Emsellem et al. 2007; Kuntschner et al. 2010), which may originate from the accretion of compact satellites able to survive disruption and that settle at the centre of the main galaxy (Balcells & Quinn 1990; but see van den Bosch et al. 2008). In the case of a disc galaxy, dynamical friction can drag a satellite to the disc plane and circularize its orbit before disruption, leaving behind a

⋆ E-mail: david@oac.uncor.edu
† Senior CIfAR Felloe.

population of co- or counterrotating disc stars, depending on the initial orbital angular momentum of the satellite (Quinn, Hernquist & Fullagar 1993; Abadi et al. 2003).

An alternative scenario envisions counterrotating stars as a result of the accretion of mainly gaseous material with angular momentum opposite that of the pre-existing stellar disc. Given its collisional nature, gas would quickly settle on to a counterrotating disc that would gradually turn into stars. The final result would be the overlap of two stellar discs sharing the same orbital plane.

How can we discriminate between these two scenarios? The gas-accretion scenario makes specific predictions about the angular momentum, spatial distribution and age difference of the two discs. Given the collisional nature of accreted gas, the two structures cannot form simultaneously, implying a well-defined age difference. Besides, since angular momentum typically correlate with accretion time (e.g. Navarro & Steinmetz 1997), one would generally expect the younger disc (accreted later) to have higher angular momentum and thus be significantly more spatially extended than the older one. Finally, it would be difficult for the pre-existing disc to avoid instabilities triggered by the counter-streaming material, which may lead to the formation of a counterrotating central bar (Palmer & Papaloizou 1990; Sellwood & Merritt 1994).

We explore these issues here using a cosmological simulation of the formation of a disc galaxy in the current paradigm of structure formation, the Λ cold dark matter (ΛCDM) scenario. The LOSVD of the simulated galaxy at $z = 0$ shows two separate peaks at positive and negative velocities, a clear signature of the presence of two disc components with opposite spins. We study their properties at the present day, and trace them back to the moment of maximum expansion (the turnaround, when their angular momenta are acquired) in order to identify the origin of this unusual configuration. We describe the numerical simulation in Section 2 and analyse its main results in Section 3. Section 4 summarizes our main conclusions.

2 THE NUMERICAL SIMULATION

The simulated galaxy analysed in this work was presented in detail by Piontek & Steinmetz (2011) where we refer the interested reader for further technical details. In brief, the simulation zooms-in on a region destined to form a galaxy-sized halo, identified in a ΛCDM simulation of a large cosmological box (64 Mpc h^{-1} on a side). The original simulation assumes the following cosmological parameters: $H_0 = 73$ km s^{-1} Mpc^{-1} (i.e. $h = 0.73$), $\sigma_8 = 0.75$, $n = 0.9$, $\Omega_0 = 0.24$ and $\Omega_\Lambda = 0.76$, adjusted to fit the *Wilkinson Microwave Anisotropy Probe* 3 results (Spergel et al. 2007). Both simulations were performed with the GADGET2 code (Springel 2005). The zoomed-in simulation splits the matter content into dark matter ($\Omega_{\rm CDM} = 0.20$) and baryons ($\Omega_{\rm b} = 0.04$), which are initially represented by gas particle that can be later converted into stars. GADGET implements the smoothed particle hydrodynamics (SPH) technique (Gingold & Monaghan 1977; Lucy 1977) to follow the hydrodynamical evolution of the gas, including pressure gradients, shocks and radiative cooling as described by Katz, Weinberg & Hernquist (1996). The star formation model follows Katz (1992) and Steinmetz & Mueller (1994, 1995), adopting a star formation rate regulated by the Schmidt (1959) law.

The gas and dark matter particle masses of the resimulation are 4.85×10^5 and $2.30 \times 10^6\,{\rm M}_\odot$, respectively. The gravitational softening is 1.03 kpc for gas, and 1.37 kpc for dark matter particles. Star particles are created with a mass $2.42 \times 10^5\,{\rm M}_\odot$, which corresponds to half that of a gas particle.

At $z = 0$, the simulated galaxy resides in a halo with a virial radius of $r_{200} = 212$ kpc (defined as the radius where the mean density contrast $\rho(<r_{200})/\rho_{\rm crit} = 200$), corresponding to a virial mass $M_{200} = 5.50 \times 10^{11}\,{\rm M}_\odot$ and to a virial velocity $V_{200} = 105$ km s^{-1}. The dimensionless spin parameter of the halo is quite low ($\lambda \sim 0.02$) and its assembly history is rather calm; its last major merger (defined by a mass ratio of 1:3 and larger) happened at a relatively high redshift, $z \sim 6$. This run corresponds to the halo identified as *DM_hr4* of the *standard* implementation of the feedback in Piontek & Steinmetz (2011) (see their tables 1 and 3).

Within the virial radius at $z = 0$, there are 160 644, 46 067 and 214 059 star, gas and dark matter particles, respectively. Most stars are confined within a smaller radius near the centre of the halo; we therefore define a 'galaxy radius', $r_{\rm gal} = 20$ kpc, which contains 150 733, 11 168 and 40 833 star, gas and dark matter particles, respectively.

3 ANALYSIS AND RESULTS

Fig. 1 shows the surface density of stars of the simulated disc galaxy at $z = 0$, projected 'face-on' (left-hand panel) and 'edge-on' (right) according to the total angular momentum of stars within $r_{\rm gal}$, which we use to define the z-axis perpendicular to the disc plane. The face-on view shows clearly the presence of a central bar, which we choose to align the y-axis of the projection.

The bar counterrotates relative to the outer disc, as shown by the LOSVD of stars in the edge-on projection. Each velocity histogram in Fig. 2 corresponds to stars projected within the small circles indicated in the right-hand panel of Fig. 1. These velocity distributions show that the inner and outer galaxies rotate in opposite directions, and that at intermediate radii the co- and counterrotating components overlap. This is reminiscent of the LOSVD of galaxies with observed counterrotating discs (see, e.g. Rix et al. 1992; Prada et al. 1996; Prada & Gutiérrez 1999).

The two components separate neatly in Fig. 3, where we show the circularity parameter, $\epsilon_J = J_z/J_{\rm circ}(E)$, of stars within $r_{\rm gal}$ as a function of binding energy, E.[1] The circularity is defined as the ratio between the Z-component of the specific angular momentum of a star and that of a circular orbit with the same binding energy (Abadi et al. 2003). It approaches unity for corotating circular orbits and -1 for counterrotating ones.

Fig. 3 shows that the outer disc has circularity approaching unity and that the bar is made up predominantly of highly bound, counterrotating ($\epsilon_J \sim -0.5$) stars. We shall hereafter consider all stars with positive or negative circularity as part of the co- or counterrotating disc, respectively. Each of these two components contributes about half of the total stellar mass within $r_{\rm gal}$. Counterrotating stars have lower energies and are more centrally concentrated; its half-mass radius is 2.4 kpc, compared to 5.9 kpc for the corotating disc.

Fig. 4, where we plot the contribution of the various components to the circular velocity profile of the galaxy, indicate that stars dominate the gravitational potential within $\sim$5 kpc. The remaining gas makes up only 10 per cent of the total baryonic matter within $r_{\rm gal}$, has a half-mass radius of 13.8 kpc, and it all corotates with the outer disc.

The main panel of Fig. 5 shows the dependence of the circularity parameter on the formation time of a star, and makes clear that the co- and counterrotating components have different ages. As

[1] Binding energies are computed using all particles within the virial radius of the halo.

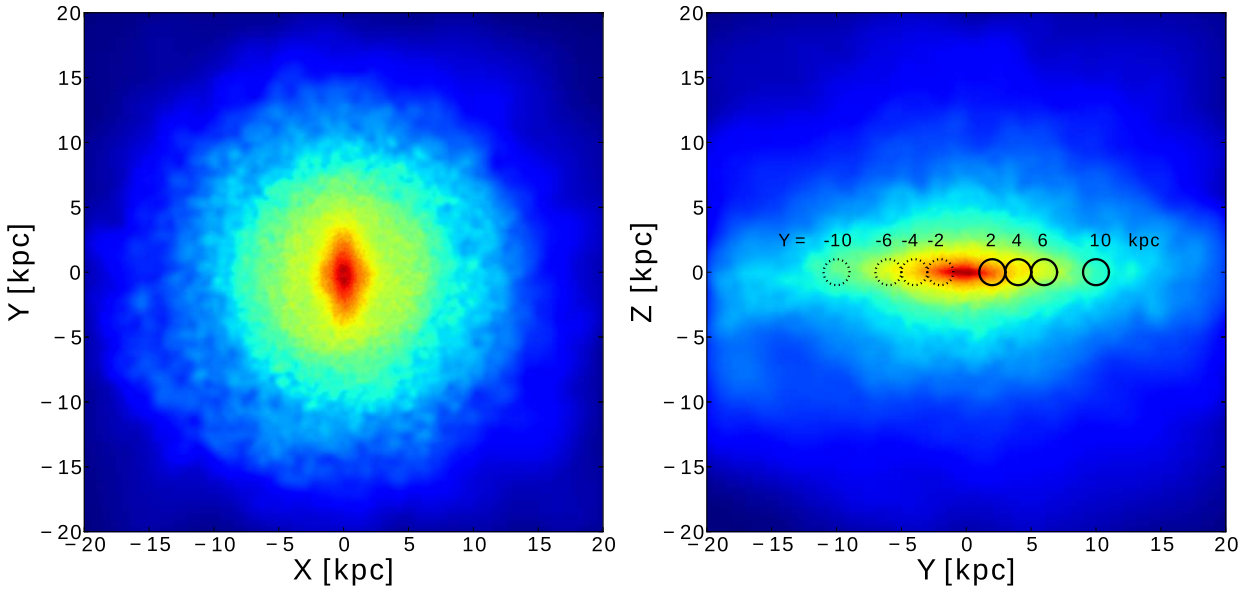

Figure 1. Face-on (left) and edge-on (right) stellar surface density maps of the simulated galaxy at $z = 0$. Note the inner bar-like structure clearly seen in the face-on view. The edge-on view shows the bar on its side. The small circles along the major axis indicate the lines of sight corresponding to the velocity distributions shown in Fig. 2.

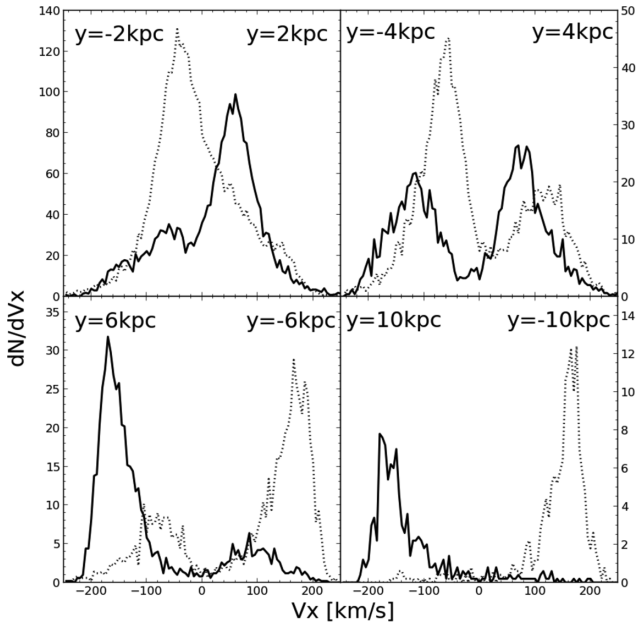

Figure 2. Velocity distributions of stars along the lines of sight indicated in the edge-on projection of the galaxy in Fig. 1. Solid and dotted curves correspond to lines of sight to the right and to the left of the centre of the galaxy, respectively. Each panel is labelled by the distance to the centre from each line of sight. Note the double peaks in the velocity distributions of the inner regions, where the lines of sight intersect the counterrotating bar-like central feature.

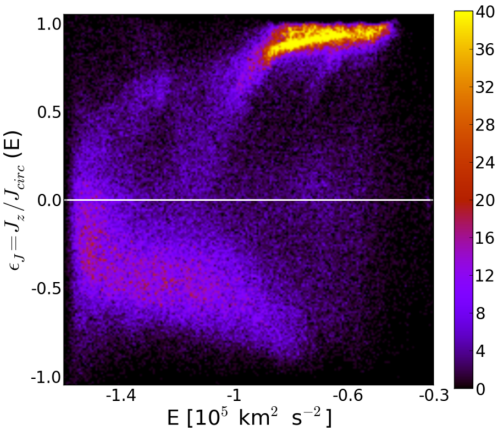

Figure 3. Circularity, $\epsilon_J = J_z/J_{\rm circ}(E)$, versus specific binding energy, E, of stars within 20 kpc from the centre of the galaxy. Colours indicate the number of stars in each pixel, following the scale on the colour bar on the right. The disc dominates in the outer regions and consists largely of particles on nearly circular orbits. The counterrotating bar-like feature dominates in the inner regions. The two components show substantial overlap in binding energy/radius.

expected, the younger component ($t_{\rm form} > 6$ Gyr) has higher angular momentum and populates the outer, corotating disc, whereas most counterrotating (bar) stars form early ($t_{\rm form} < 6$ Gyr).

The presence of the bar (which grows gradually after $t = 6$ Gyr and is fully formed by $t = 9$ Gyr) has interesting effects on the orbits of co- and counterrotating stars. We study this by dividing them into three subgroups each according to their age: $t_{\rm form} < 3$ Gyr, 3 Gyr $< t_{\rm form} < 6$ Gyr and $t_{\rm form} > 6$ Gyr (see the six regions outlined in Fig. 5). Fig. 6 shows the spatial distribution of each of these subcomponents as seen in a face-on view of the galaxy. The oldest two (regions 1 and 2) form a central 'bulge' that is affected little by the bar and that contains most of the accreted stars.

Fig. 6 also shows that even corotating stars contribute to the bar pattern; indeed, stars in region 3 follow closely the bar pattern even though they rotate in *opposite* sense to that of most stars in the bar, as predicted by theory (e.g. Zhao 1996; Wozniak & Pfenniger 1997). Young stars (regions 5 and 6) define the main sense of rotation of the galaxy, but their spatial distribution reveals that their orbits are significantly affected by the bar. Note, for example, the 'ring' feature at $R \sim 6$ kpc visible in region 5, and the presence of two overdense regions of stars along a direction perpendicular to

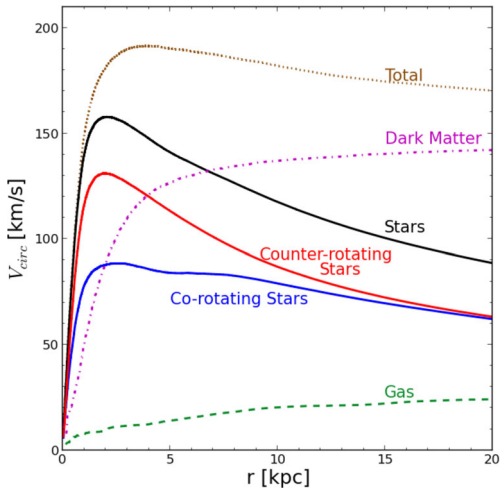

Figure 4. Contribution to the circular velocity profile of the different components. Note that stars dominate in the inner ∼7 kpc and that the co- and counterrotating stellar components have approximately the same mass. The circular velocity profile is nearly flat, with the dark matter dominating the outer regions. The gas makes up less than 10 per cent of the total baryonic mass within 20 kpc.

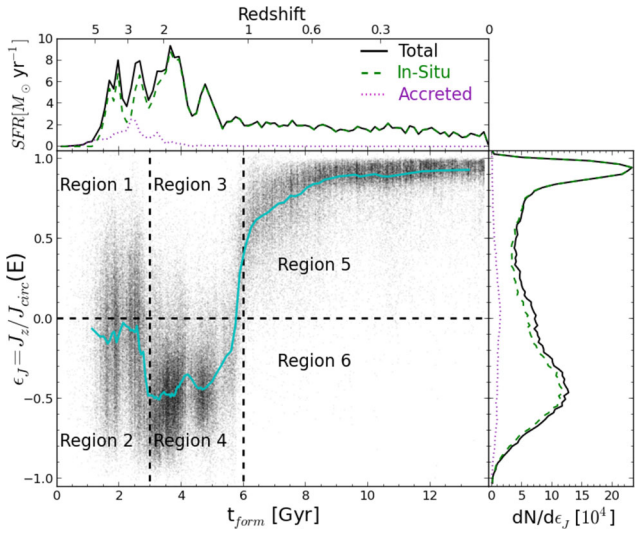

Figure 5. Main panel: circularity ($\epsilon_J = J_z/J_{\rm circ}(E)$) as function of formation time, $t_{\rm form}$, for stars within 20 kpc from the centre of the galaxy at $z = 0$. The cyan curve indicates the median ϵ_J as a function of $t_{\rm form}$. Note the sharp age difference between the co- and counterrotating stellar components. Top panel: distribution of star formation times, split by stars formed in situ (i.e. in the main progenitor) and those accreted from satellites. The vast majority of stars (91 per cent) in the galaxy were formed in situ. Right-hand panel: Distribution of circularities of stars shown in the main panel.

the bar (at $X \sim \pm 2$ kpc). These patterns likely correspond to the location of resonances in the prograde disc with the counterrotating bar potential, highlighting a complex dynamical situation which we plan to study in detail in a future contribution. We turn our attention now to the origin of the co- and counterrotating discs.

As discussed above, counterrotating stars are mainly ∼6 Gyr old or older, and some of them have been accreted from different progenitors. The latter population, however, make up only a small fraction, 9 per cent, of the stellar mass of the galaxy. Indeed, both the co- and counterrotating discs are made up primarily of stars formed in situ and, given their spatial overlap, must differ in their formation time. This suggests that the origin of these two components is linked to differences in the angular momentum of the accreting gas which, at late times, flows with a net spin opposite to that of the pre-existing galaxy.

What causes the change in spin direction of the accreting gas? We look for clues in the temporal evolution of the two components, going back to the time of maximum expansion (i.e. turnaround), when their net angular momentum was acquired. To this aim, we computed the evolution of the angular momentum of the baryons making up each of the two components as a function of time, in the reference frame of the main galaxy progenitor. As reported in earlier work (see, e.g. Navarro & Steinmetz 1997; Abadi et al. 2010), the angular momentum of each component rises quickly with time until turnaround and stays roughly constant or declines slightly thereafter.

Interestingly, at turnaround ($z_{\rm ta} = 2.12$) the two components already had opposite spins, implying that something in the torquing process that endows each component with net rotation is responsible for the origin of the two components. We show this in Fig. 7, where we plot the spatial configuration of all particles in a 1.2 Mpc (physical) box centred on the galaxy main progenitor at $z_{\rm ta}$. We highlight in yellow the baryons that at $z = 0$ will be found within the galaxy radius, $r_{\rm gal}$, and plot them in a Cartesian (x,y,z) reference frame aligned with the principal axes of their inertia tensor (x and z correspond to the major and minor axis, respectively). Roughly 90 per cent of all baryons destined to form the galaxy are contained at $z_{\rm ta} = 2.12$ within the cyan circle shown in the left-hand panels of Fig. 7, and about half of them are found within the magenta circle. With few exceptions, baryons within the inner magenta circle contribute to the counterrotating component at $z = 0$; those outside it make up primarily the outer disc. The inner baryons collapse to form a stellar disc which, after the accretion of the outer component, turns into the counterrotating bar seen at $z = 0$.

Arrows in the left-hand panels of Fig. 7 indicate the direction of the torque operated on each of the inner (magenta) or outer (cyan) baryons by external material (i.e. that outside the cyan circle). They clearly point in opposite directions (∼130°), mainly along the y (intermediate) axis of the projection, as expected from tidal torque theory. Indeed, the component of the torque along one axis, $\tau_i \approx T_{jk}(I_{jj} - I_{kk})$ ($i \neq j \neq k$ and run from 1 to 3), scales to first order as the difference of the inertia moments of the other two axes: τ_i is therefore generally largest along the intermediate axis. (Here, $T_{ij} = \partial^2\phi/\partial x_i \partial x_j$ is the tidal tensor generated by external material. The calculation assumes a reference frame where the inertia tensor is diagonal; see Navarro, Abadi & Steinmetz 2004b for details.)

The reason for the switch in the direction of the torque operating on the inner/outer galaxy becomes clear once we realize that the accreted gas is channelled towards the galaxy primarily along two large-scale filaments: one, which we label 'Filament 1', is aligned with the positive x-axis of Fig. 7 and a second one, which we call 'Filament 2', traces the diagonal of the $(-x,-y,-z)$ octant. The galaxy forms roughly at the 'V'-like intersection of these two filaments: Filament 1 contributes most of the material of the outer galaxy, while the baryons making up the counterrotating inner galaxy flow mainly along Filament 2.

The right-hand panels of Fig. 7 present a simplified model that attempts to mimic the external mass distribution responsible for torquing the material destined to be accreted into the galaxy. We represent the inner (magenta) and outer (cyan) galaxy material at turnaround as triaxial ellipsoids whose major axis is aligned with that of each filament. The axial ratios of the ellipsoids are $(b/a = 0.93, c/a = 0.70)$ and $(b/a = 0.82, c/a = 0.41)$ for the inner and outer galaxy material, respectively. These values, together with

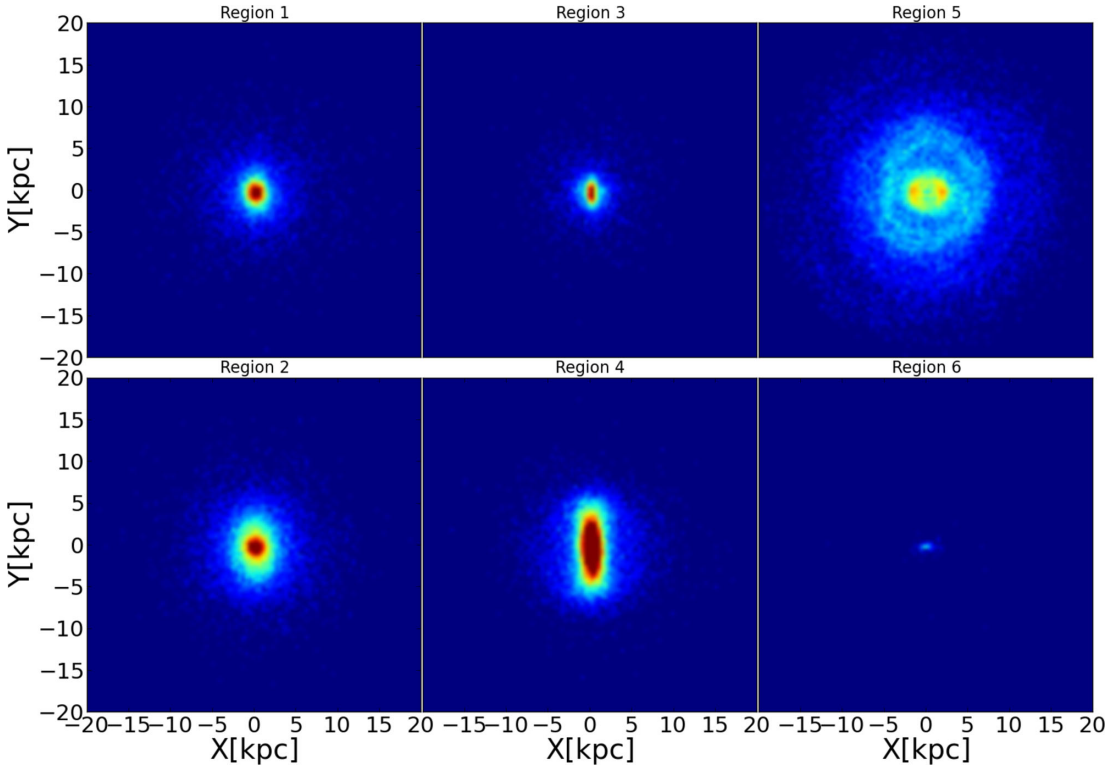

Figure 6. As Fig. 1, but for stars in the six regions defined in Fig. 5. Note that the counterrotating bar has many particles with positive circularities (region 3). Note as well the dynamical features (rings, overdensities) in the corotating disc caused by the counterrotating bar potential.

their orientations, are adopted to match closely those of the inertia tensor of the inner and outer material at that time.

The filaments themselves are represented in the model by $10^{11}\,M_{\odot}$ one-dimensional mass distributions that extend out to 600 kpc from the centre, and are aligned as indicated in the right-hand panels of Fig. 7. Because the principal axes of the inner galaxy material are aligned with Filament 2, it can only be torqued by Filament 1. Analogously, the outer galaxy material can only be torqued by Filament 2. This arrangement produces torques of roughly opposite signs on the inner and outer galaxy, which are shown by the arrows in the right-hand panels of Fig. 7, and results in perfectly anti-aligned spins at $z = 0$. Note that the directions and relative magnitudes of the components of the torque in the model (right-hand panels) are in very good agreement with those actually measured in the simulation for the inner and outer galaxy (left-hand panels).

We conclude that the counterrotating components originate from the peculiar torquing process that arises from the accretion of gas along two different filaments that intersect in a 'V'-like configuration at the time of turnaround. The material that flows into the galaxy along one filament is naturally torqued in a direction opposite to that of material accreting along the other. This would not necessarily result in a two-component disc; if accretion along both filaments was coeval then the collisional nature of the gas would ensure that only one disc forms. In the case of our simulated galaxy, however, enough time separates the two episodes of accretion to allow the stellar component of the inner galaxy to form before the accretion of the material that forms the outer disc occurs.

4 SUMMARY AND CONCLUSIONS

We explore the origin of counterrotating stars in disc galaxies whose orbits are confined to the plane of the disc. This is a puzzling dynamical feature known to be present in a number of disc galaxies, but its origin, be it mergers, secular evolution or external gas accretion, is still under debate. We show here that this configuration arises without fine tuning in a simulation of galaxy formation in a ΛCDM universe and may therefore offer interesting insight into its origin. Most stars in the simulation are formed in situ, and mergers play no significant role in the formation of the disc.

The co- and counterrotating components have distinct ages and, despite some overlap, show differences in their spatial distributions. We show that they actually arise from separate episodes of infall of gas with opposite spins. The spin reversal may be traced to the fact that the galaxy forms at the end of two intersecting filaments which, at turnaround (when their net angular momentum is acquired), form a 'V'-like configuration. One filament provides the early-collapsing material that forms the stars of the inner galaxy while the outer galaxy material is supplied by the other. Each filament torques material on the other filament but not on its own, leading to the acquisition of opposite spins before collapse. The early-collapsing material is able to form an inner stellar disc before the second episode of accretion results in the formation of a more extended disc that rotates in the opposite direction.

Since filamentary gas accretion is commonplace in ΛCDM, one may wonder why counterrotating stars are not more prevalent in disc galaxies than observed. One reason is that a number of conditions are required to form stellar discs with counterrotating components. Although accretion along filaments is quite common in ΛCDM, the 'V'-like configuration at turnaround that leads to opposite spins is much less frequent. In addition, the accretion from one and the other filament must be timed to allow for the two stellar components to form one before the other is accreted, again a condition that would be satisfied only in a minority of cases.

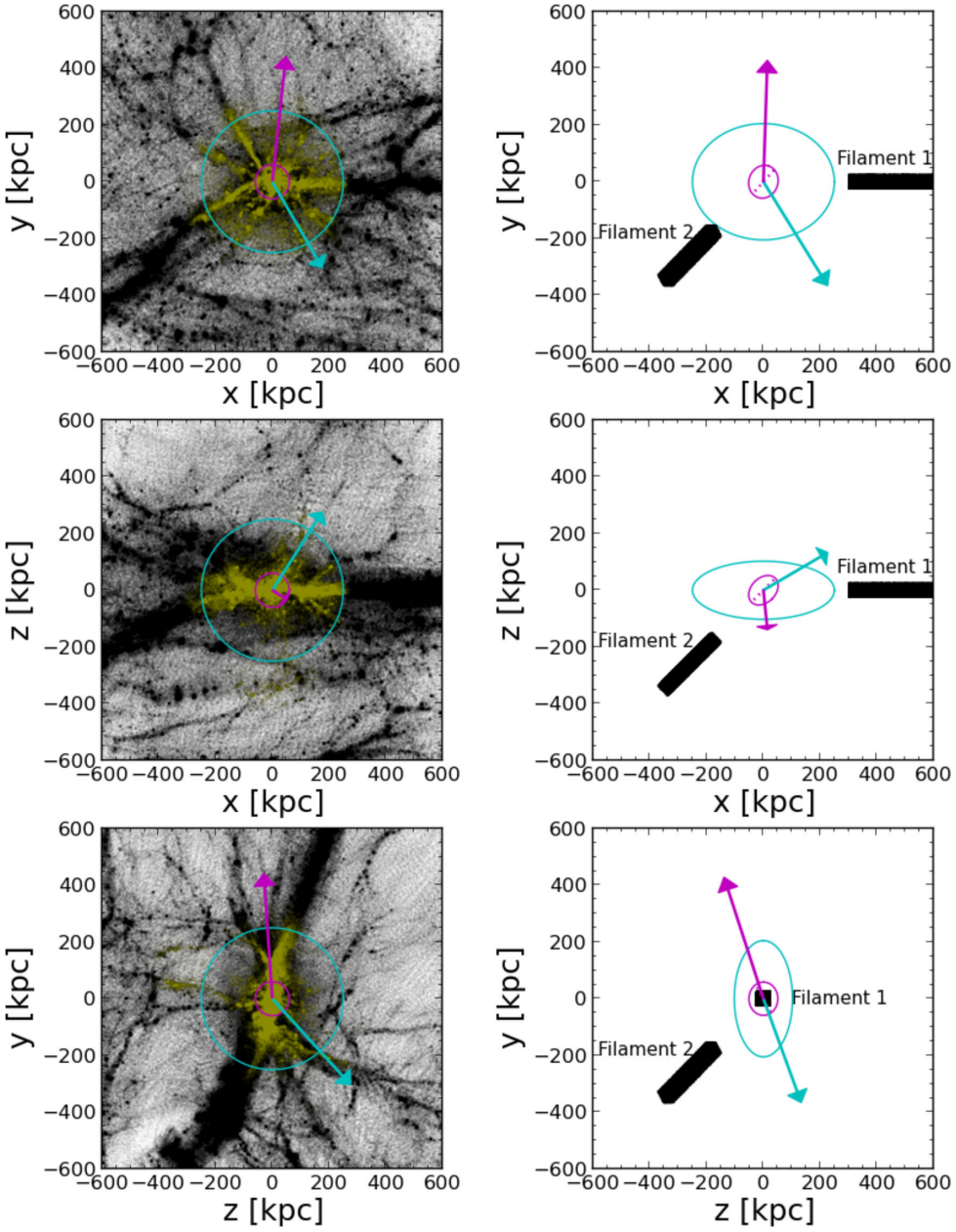

Figure 7. Left-hand panels: spatial distribution of all the mass (black dots) and the baryons destined to form the galaxy at $z = 0$ (yellow dots) at $z_{\rm ta} = 2.12$ inside a box of 1.2 Mpc (physical). The cyan and magenta circles contain 90 and 45 per cent of all yellow particles, respectively. Material within the outer/inner circle contributes mostly to the co- and counterrrotating disc at $z = 0$. Arrows show the orientation of the torque vector due to the external material operating on the baryonic particles inside the circles of each respective colour, as measured in the simulation. Note that the torque on the inner/outer galaxy points in nearly opposite directions. Right-hand panels: toy model of the mass distribution shown in the left-hand panels. The filaments represent the particles which generate the external tides. Magenta and cyan ellipsoids indicate the shape and orientation of the material that will form the inner and outer galaxy, respectively. Arrows indicate the tidal torque vector exerted by the external mass distribution, as measured in the model. Note the excellent agreement between the orientation of the tidal torque vector in the right- and left-hand panels.

We conclude that the accretion of gas with spin misaligned relative to the pre-existing galaxy might be responsible for at least some of the counterrotating stars in disc galaxies, especially those where such stars differ in age and spatial distribution from the main disc. These spin misalignments arise naturally in a hierarchically clustering scenario, where net angular momentum results from the coupling between the tidal stress tensor and the inertia tensor of the material destined to form a galaxy at early times (see, e.g. Navarro et al. 2004a). Differences in the spatial distribution of early- and late-accreting material at early times can therefore result in large differences in the direction of their acquired spin.

Such misalignments may play a more significant role in galaxy formation than is usually recognized. Indeed, they may not only explain morphological and dynamical oddities such as counterrotating disc stars and polar rings (e.g. Macciò, Moore & Stadel 2006) but may also play a substantial role in the formation of spheroidal galaxies. Indeed, Scannapieco et al. (2009) and Sales et al. (2012) have argued that many stellar spheroids may result not from mergers

but rather from the overlap of several episodes of gaseous accretion with misaligned spins. Although each episode leaves behind a population of stars with a well-defined age and spin the ensemble may be indistinguishable from a slowly rotating elliptical galaxy. Further work should help to clarify whether the vast diversity of galaxy morphologies is indeed linked to the complex patterns of gas accretion in a hierarchically clustering universe, as these simulations suggest.

ACKNOWLEDGEMENTS

We thank the referee, Professor Hervé Wozniak, for a prompt and very constructive report. We also thank Alejandro Benitez Llambay for his code PY-SPHVIEWER.

REFERENCES

Abadi M. G., Navarro J. F., Steinmetz M., Eke V. R., 2003, ApJ, 597, 21
Abadi M. G., Navarro J. F., Fardal M., Babul A., Steinmetz M., 2010, MNRAS, 407, 435
Balcells M., Quinn P. J., 1990, ApJ, 361, 381
Bender R., Surma P., 1992, A&A, 258, 250
Bertola F., Cinzano P., Corsini E. M., Pizzella A., Persic M., Salucci P., 1996, ApJ, 458, L67
Carter D., Thomson R. C., Hau G. K. T., 1998, MNRAS, 294, 182
Coccato L., Morelli L., Corsini E. M., Buson L., Pizzella A., Vergani D., Bertola F., 2011, MNRAS, 412, L113
Emsellem E. et al., 2007, MNRAS, 379, 401
Gingold R. A., Monaghan J. J., 1977, MNRAS, 181, 375
Katz N., 1992, ApJ, 391, 502
Katz N., Weinberg D. H., Hernquist L., 1996, ApJS, 105, 19
Kuntschner H. et al., 2010, MNRAS, 408, 97
Lucy L. B., 1977, AJ, 82, 1013
Macciò A. V., Moore B., Stadel J., 2006, ApJ, 636, L25
Merrifield M. R., Kuijken K., 1994, in Sato K., ed., Proc. 37th Yamada Conf. Evolution of the Universe and its Observational Quest. IoP Publishing, Bristol, p. 491
Navarro J. F., Steinmetz M., 1997, ApJ, 478, 13
Navarro J. F. et al., 2004a, MNRAS, 349, 1039
Navarro J. F., Abadi M. G., Steinmetz M., 2004b, ApJ, 613, L41
Palmer P. L., Papaloizou J., 1990, MNRAS, 243, 263
Piontek F., Steinmetz M., 2011, MNRAS, 410, 2625
Prada F., Gutiérrez C. M., 1999, ApJ, 517, 123
Prada F., Gutierrez C. M., Peletier R. F., McKeith C. D., 1996, ApJ, 463, L9
Quinn P. J., Hernquist L., Fullagar D. P., 1993, ApJ, 403, 74
Rix H.-W., Franx M., Fisher D., Illingworth G., 1992, ApJ, 400, L5
Rubin V. C., Graham J. A., Kenney J. D. P., 1992, ApJ, 394, L9
Sales L. V., Navarro J. F., Theuns T., Schaye J., White S. D. M., Frenk C. S., Crain R. A., Dalla Vecchia C., 2012, MNRAS, 423, 1544
Scannapieco C., White S. D. M., Springel V., Tissera P. B., 2009, MNRAS, 396, 696
Schmidt M., 1959, ApJ, 129, 243
Sellwood J. A., Merritt D., 1994, ApJ, 425, 530
Spergel D. N. et al., 2007, ApJS, 170, 377
Springel V., 2005, MNRAS, 364, 1105
Steinmetz M., Mueller E., 1994, A&A, 281, L97
Steinmetz M., Mueller E., 1995, MNRAS, 276, 549
van den Bosch R. C. E., van de Ven G., Verolme E. K., Cappellari M., de Zeeuw P. T., 2008, MNRAS, 385, 647
Vergani D., Pizzella A., Corsini E. M., van Driel W., Buson L. M., Dettmar R.-J., Bertola F., 2007, A&A, 463, 883
Wozniak H., Pfenniger D., 1997, A&A, 317, 14
Zhao H., 1996, MNRAS, 283, 149

This paper has been typeset from a TEX/LATEX file prepared by the author.